

Controlled Dopant Distribution and Higher Doping Efficiencies by Surface-Functionalized Atomic Layer Deposition

Angel Yanguas-Gil, Kyle E. Peterson, and Jeffrey W. Elam*

Energy Systems Division, Argonne National Laboratory, 9700 South Cass Avenue, Argonne Illinois 60439, United States

S Supporting Information

KEYWORDS: surface functionalization, growth inhibition, atomic layer deposition, doping control, Al₂O₃, ZnO, TiO₂

The physical properties of doped thin films depend on the dopant concentration as well as the position, bonding, and spatial distribution of the dopants, which dictate the fraction of active dopant atoms (the doping efficiency).^{1,2} Unfortunately, most thin film deposition techniques provide little or no control over the dopant distribution. For instance, atomic layer deposition (ALD) provides precise control over the average dopant concentration due to its digital, self-limited nature, but the layer-by-layer growth limits spatial control to the direction of growth.^{3,4} This limitation stems from the fact that the number of dopant atoms deposited per layer in the host material is controlled by the ALD saturation coverage, which is a fixed value for every precursor/coreactant/host combination. This produces strongly inhomogeneous doping profiles even for low dopant concentrations and can lead to lower doping efficiencies through dopant clustering.⁵ Previous attempts to alleviate this problem employed ALD precursors with a lower growth per cycle⁴ and subsaturating dopant precursor exposures.⁶ Although both methods provide some benefit, the first is inconvenient because it requires evaluating new precursors for each dopant/host system, and the second method can lead to poor thickness homogeneity and reduced conformality. In this work, we introduce a very general method for controlling the dopant spatial distribution yielding increased doping efficiencies without sacrificing film conformality.

In our approach, the conventional precursor/coreactant ALD sequence is preceded by a surface functionalization step that reduces the density of surface reactive sites. As a result, the subsequent precursor exposure deposits fewer surface species. The coreactant exposure then removes the functionalization groups and restores the initial surface so that the cycle can be repeated. This functionalization/precursor/coreactant sequence effectively allows controlled, submonolayer saturation coverages.

The chemical species used for surface functionalization in ALD must satisfy certain requirements: (i) they must bond strongly enough to survive the purging times between exposures; (ii) they must infiltrate high aspect ratio features to preserve the conformality of ALD; (iii) they must resist displacement during the precursor exposures; and (iv) they must be completely removed during the coreactant exposures.

Alkyl alcohols are promising candidates for surface functionalization on metal oxide surfaces. Previous work showed that alkyl alcohols react on metal oxides to form stable alkoxide or alkoxylate species that can be readily displaced by H₂O.^{7,8}

Furthermore, grafted alkyl alcohols appear to inhibit ALD. For example, surface poisoning by isopropanol (ⁱPrOH) released during the dissociative adsorption of titanium tetraisopropoxide (TTIP) on TiO₂ was suspected as the cause for the reduced TiO₂ growth per cycle.⁹

To evaluate the viability of alkyl alcohols for surface functionalization, we performed in situ quartz crystal microbalance (QCM) studies in a viscous flow ALD reactor.¹⁰ These experiments were conducted at 200 °C unless indicated otherwise. Our initial measurements examined the reaction of ethanol (EtOH) on Al₂O₃ and TiO₂ surfaces prepared in situ by ALD using Al(CH₃)₃ (TMA) and titanium tetrachloride (TiCl₄), respectively, with H₂O as the coreactant. Figure 1a shows that when these surfaces were subjected to alternating 1s, 0.1 Torr exposures of EtOH and H₂O separated by 5s purge periods, the mass increased during the EtOH exposures and decreased during the H₂O exposures. During the purge times between pulses the mass remained constant.

In situ mass spectrometry (MS) signals recorded concurrently with the QCM measurements showed an intensity increase for mass fragment $m/z = 31$ (attributed to CH₂OH⁺, the dominant crack of EtOH) during the H₂O pulses after an EtOH pulse (see Figure S1 in the Supporting Information). In contrast, repeated exposures to just H₂O caused the $m/z = 31$ signal intensity to drop to background levels. When D₂O was substituted for H₂O as the coreactant, the $m/z = 19$ (DOH⁺) intensity increased during the ethanol pulses while the $m/z = 32$ (CH₂OD⁺) signal increased during the subsequent D₂O pulses. The combined QCM and MS results suggest that EtOH adsorbs dissociatively onto the Al₂O₃ and TiO₂ surfaces displacing H₂O and the subsequent H₂O exposures displace the EtOH.¹¹

The effect of EtOH surface functionalization on Al₂O₃ ALD is revealed by the in situ QCM data in Figure 1b. The first two cycles show conventional Al₂O₃ ALD using TMA/H₂O. This process deposits 37 ng/cm²/cycle and yields the familiar staircase pattern comprised of a mass increase during the TMA exposures and essentially no net mass change from the H₂O exposures.¹² In contrast, the EtOH/TMA/H₂O sequence yields only 16 ng/cm²/cycle and generates a smaller mass increase during the TMA exposures compared to the conventional ALD

Received: May 23, 2011

Revised: August 2, 2011

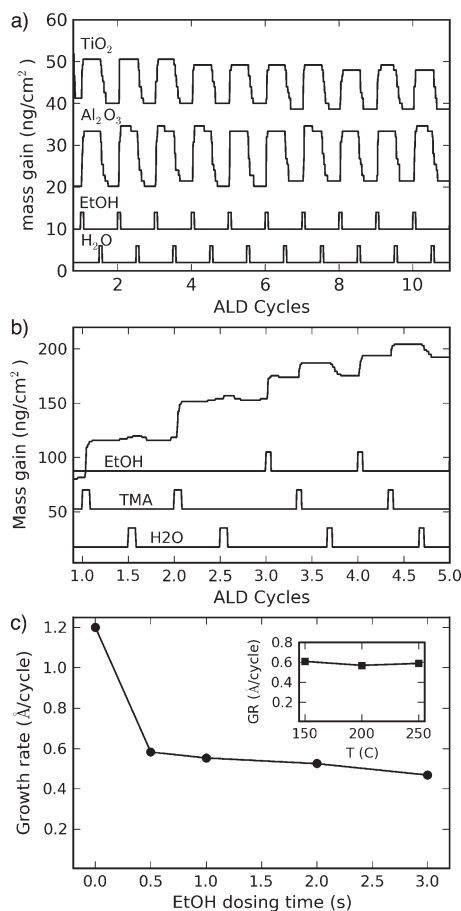


Figure 1. (a) QCM mass signals during alternating EtOH/H₂O exposures on Al₂O₃ and TiO₂; (b) QCM mass signals during Al₂O₃ growth using TMA/H₂O and EtOH/TMA/H₂O exposure sequences; (c) influence of EtOH exposure time and growth temperature (inset) on Al₂O₃ growth per cycle using the EtOH/TMA/H₂O sequence.

and a mass decrease during the H₂O exposures. Extending the TMA exposure time following the EtOH exposure did not increase the Al₂O₃ growth per cycle, and MS measurements showed that no EtOH ($m/z = 31$) was released during the TMA exposures. Our explanation for the inhibited Al₂O₃ growth is that EtOH displaces surface hydroxyls and blocks potential adsorption sites for the TMA. Consequently, the TMA exposures deposit fewer Al(CH₃)_x species and the Al₂O₃ growth is reduced. TMA does not react with the ethoxide blocking agents, but they are removed during the H₂O exposures allowing the Al₂O₃ ALD to proceed.

Figure 1c demonstrates that the EtOH functionalization is self-limiting because increasing the EtOH exposure time beyond ~0.5s did not substantially change the Al₂O₃ growth per cycle. Furthermore, the inset of Figure 1c shows that the inhibition is nearly temperature independent in the range considered. These findings suggest that surface-functionalized ALD should preserve the excellent conformality and uniformity of conventional ALD. Indeed, the thicknesses of Al₂O₃ films prepared using surface functionalized ALD were extremely uniform ($\pm 0.5\%$) along the entire 40 cm length of the ALD reactor (see Figure S2 in the Supporting Information).

Careful inspection of the QCM data reveals an apparent discrepancy in our proposed mechanism. In Figure 1a, the mass

Table 1. Effect of Alkyl Alcohol Functionalization on Metal Oxide ALD Growth Per Cycle Using H₂O As the Oxygen Source^a

	TMA	DEZ	TiCl ₄	TTIP
MeOH	0.40	0.33	0.26	0.22
EtOH	0.48	0.47	0.39	0.26
ⁱ PrOH	0.52	0.58	0.60	0.26

^a Values are normalized to the growth per cycle without functionalization.

gains during the EtOH exposures equal the mass losses from the following H₂O exposures. However, in Figure 1b, the mass gains during the EtOH exposures are larger than the corresponding mass losses during the H₂O exposures. One explanation is that the TMA does in fact displace some EtOH species. MS seems to rule out this possibility since no EtOH was evolved during the TMA exposures. Also, the growth per cycle is self-limited with respect to the TMA dose time. Therefore, any partial exchange must have fast self-limited kinetics. Another possibility is that the unexpectedly large mass increases during the EtOH exposures in Figure 1b result from EtOH adsorption on some Al₂O₃ surface sites (e.g., Al–O–Al bridge sites) without releasing H₂O. In support of this idea, the first EtOH exposure on a fresh ALD Al₂O₃ surface always produced a larger mass gain than the subsequent EtOH exposures during repeated EtOH/H₂O cycles (see Figure S3 in the Supporting Information).

Our in situ measurements during the surface-functionalized Al₂O₃ ALD suggest that TMA does not react with the surface alkoxide species. This is somewhat surprising given that alkyl alcohols have been used previously as the oxygen source during Al₂O₃ ALD.^{13–16} One difference between our experiments and these previous studies is that they used higher growth temperatures of 250–600 °C, and it is likely that these higher temperatures are needed to break the R–O bonds in the ROH molecules to facilitate growth. Indeed, when we performed alternating TMA/ROH exposures (R = Et, ⁱPr) at 200 °C, we observed no mass changes by QCM. Another difference is that these previous experiments used TMA/ROH cycles, which exposed the TMA-saturated surface to ROH vapor, whereas in surface-functionalized ALD using ROH/TMA/H₂O cycles this is not the case, so the surface chemistry might not be the same.

To further investigate the growth inhibition observed by QCM we deposited a range of ALD metal oxide films on silicon substrates using different alkyl alcohols and various metal precursors and measured the film thicknesses by ex situ ellipsometry. Table 1 shows the growth per cycle values deduced from these measurements normalized to the corresponding values without the surface functionalization (see Figure S5 in the Supporting Information). Table 1 shows that the degree of inhibition is higher for MeOH than for EtOH and ⁱPrOH. One hypothesis is that the lower pK_a of MeOH compared to the other alcohols leads to a higher surface coverage¹⁷ and more effective poisoning. However, the pK_a differences between MeOH, EtOH, and ⁱPrOH are too small to account for the differences observed in the degree of inhibition. Furthermore, Benaissa et al showed that MeOH and ⁱPrOH exhibit similar chemisorption behavior on γ -Al₂O₃,¹⁷ and Suda et al. measured almost identical surface coverages for the irreversible absorption of MeOH, EtOH, and PrOH on polycrystalline rutile TiO₂ surfaces.⁸ It is interesting to note that the inhibition of titanium tetraisopropoxide is much

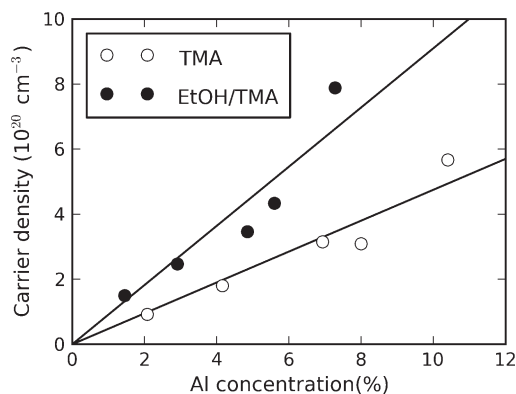


Figure 2. Free carrier concentration as a function of the Al atomic percent in Al:ZnO films. Solid lines show linear fits to the carrier density for the films prepared using conventional ALD (open circles, slope = 0.47) and surface-functionalized ALD (closed circles, slope = 0.91).

greater than that of TiCl_4 for each of the three alkyl alcohols (Table 1). Evidently, the inhibition depends not only on the surface coverage of the functional moiety, but also on the overlap between the sites that are functionalized and those that are reactive toward the precursor.

To confirm the reversibility of the surface functionalization, we deposited Al_2O_3 using the sequence EtOH/ H_2O /TMA/ H_2O and, as expected, no inhibition was observed. Depth-profiling X-ray photoelectron spectroscopic analysis detected no carbon impurities (detection limit 0.5 at%) in Al_2O_3 and ZnO films prepared using surface functionalization, indicating that the alkoxide species were completely displaced by the H_2O (see Figure S4 in the Supporting Information). Likewise, the optical properties of these films derived from ex-situ spectroscopic ellipsometry were identical with and without the surface functionalization (see Figure S5 in the Supporting Information).

Finally, to demonstrate the utility of growth inhibition through surface functionalization, we used this technique to deposit Al-doped ZnO (Al:ZnO). Al:ZnO is a transparent conducting material and an n-doped degenerate semiconductor upon Al substitutional doping of the Zn sites.¹⁸ We varied the Al doping by executing supercycles consisting of N ZnO ALD cycles followed by 1 Al_2O_3 ALD cycle using $N = 9, 12, 14, 24$, and 49.¹⁹ We prepared films with and without EtOH surface functionalization prior to the TMA dose. The Al concentrations were determined by X-ray fluorescence measurements and the carrier densities were evaluated using Hall probe measurements. As expected, we measured a lower Al concentration for a given N value as a result of the growth inhibition (Figure 2). Remarkably, however, the Al:ZnO films prepared using surface functionalization exhibited carrier concentrations 2× higher on average than conventional ALD films of similar Al concentration. This increased doping efficiency is a direct consequence of the more efficient distribution of dopants in the ZnO host. The lower Al packing density afforded by surface-functionalized ALD reduces the probability of forming Al–O–Al clusters that do not act as donors.

Extending this methodology to species other than alkyl alcohols should permit a wider range of saturation coverages with correspondingly greater dopant spatial control. Furthermore, this could enable the selective blocking of chemically distinct surface sites. This technique could also be applied to other classes of ALD materials and might provide control over the nucleation of ALD thin films and nanoparticles.

ASSOCIATED CONTENT

S Supporting Information. Mass spectrometry, XPS depth profiles, spectroscopic ellipsometry data. This material is available free of charge via the Internet <http://pubs.acs.org>

AUTHOR INFORMATION

Corresponding Author

*E-mail: jelam@anl.gov.

ACKNOWLEDGMENT

This work was supported by the U.S. DOE, EERE-Industrial Technologies Program under FWP-4902A. The in situ analysis was supported as part of the Argonne-Northwestern Solar Energy Research (ANSER) Center, an Energy Frontier Research Center funded by the U.S. Department of Energy, Office of Science, Office of Basic Energy Sciences under Award DE-SC0001059.

REFERENCES

- (1) Kostlin, H.; Jost, R.; Lems, W. *Phys. Status Solidi A Research* **1975**, *29* (1), 87–93.
- (2) Polman, A. *J. Appl. Phys.* **1997**, *82* (1), 1–39.
- (3) Na, J. S.; Peng, Q.; Scarel, G.; Parsons, G. N. *Chem. Mater.* **2009**, *21* (23), 5585–5593.
- (4) Van, T. T.; Chang, J. P. *Appl. Phys. Lett.* **2005**, *87* (1), 011907.
- (5) Na, J. S.; Scarel, G.; Parsons, G. N. *J. Phys. Chem. C* **2010**, *114* (1), 383–388.
- (6) Lee, D. J.; Kwon, J. K.; Kim, H. M.; Kim, H. S.; Kim, K. B. In *AVS Topical Conference on Atomic Layer Deposition ALD 2010*; Seoul, Korea, June 21–23, 2010; American Vacuum Society: New York, 2010.
- (7) Evans, H. E.; Weinberg, W. H. *J. Chem. Phys.* **1979**, *71* (4), 1537–1542.
- (8) Suda, Y.; Morimoto, T.; Nagao, M. *Langmuir* **1987**, *3* (1), 99–104.
- (9) Ritala, M.; Leskela, M.; Niinisto, L.; Haussalo, P. *Chem. Mater.* **1993**, *5* (8), 1174–1181.
- (10) Elam, J. W.; Groner, M. D.; George, S. M. *Rev. Sci. Instrum.* **2002**, *73* (8), 2981–2987.
- (11) Kim, K. S.; Barteau, M. A.; Farneth, W. E. *Langmuir* **1988**, *4* (3), 533–543.
- (12) Puurunen, R. L. *J. Appl. Phys.* **2005**, *97* (12), 121301.
- (13) Woo-Seok, J.; Sung, Y.; Choon-soo, L.; Sang-Won, K. *J. Electrochem. Soc.* **2002**, *149* (6), C306–C310.
- (14) Sammelselg, V.; Tarre, A.; Lu, J.; Aarik, J.; Niilisk, A.; Uustare, T.; Netsipailo, I.; Rammula, R.; Parna, R.; Rosental, A. *Surf. Coat. Technol.* **2010**, *204* (12–13), 2015–2018.
- (15) Cheng-Wei, C.; Eugene, A. F. *Appl. Phys. Lett.* **2008**, *93* (3), 031902.
- (16) Clavel, G.; Rauwel, E.; Willinger, M. G.; Pinna, N. *J. Mater. Chem.* **2009**, *19* (4), 454–462.
- (17) Benaissa, M.; Saur, O.; Lavalley, J. C. *Mater. Chem.* **1982**, *7* (5), 699–714.
- (18) Ellmer, K. *J. Phys. D: Appl. Phys.* **2001**, *34* (21), 3097–3108.
- (19) Elam, J. W.; George, S. M. *Chem. Mater.* **2003**, *15* (4), 1020–1028.